

# UC Irvine

## UC Irvine Previously Published Works

### Title

Subaqueous melting of Store Glacier, west Greenland from three-dimensional, high-resolution numerical modeling and ocean observations

### Permalink

<https://escholarship.org/uc/item/3qs55782>

### Journal

Geophysical Research Letters, 40(17)

### ISSN

0094-8276

### Authors

Xu, Yun  
Rignot, Eric  
Fenty, Ian  
[et al.](#)

### Publication Date

2013-09-16

### DOI

10.1002/grl.50825

### Copyright Information

This work is made available under the terms of a Creative Commons Attribution License, available at <https://creativecommons.org/licenses/by/4.0/>

Peer reviewed

# Subaqueous melting of Store Glacier, west Greenland from three-dimensional, high-resolution numerical modeling and ocean observations

Yun Xu,<sup>1</sup> Eric Rignot,<sup>1,2</sup> Ian Fenty,<sup>2</sup> Dimitris Menemenlis,<sup>2</sup> and M. Mar Flexas<sup>2</sup>

Received 2 May 2013; revised 26 July 2013; accepted 1 August 2013; published 4 September 2013.

[1] We present three-dimensional, high-resolution simulations of ice melting at the calving face of Store Glacier, a tidewater glacier in West Greenland, using the Massachusetts Institute of Technology general circulation model. We compare the simulated ice melt with an estimate derived from oceanographic data. The simulations show turbulent upwelling and spreading of the freshwater-laden plume along the ice face and the vigorous melting of ice at rates of meters per day. The simulated August 2010 melt rate of  $2.0 \pm 0.3$  m/d is within uncertainties of the melt rate of  $3.0 \pm 1.0$  m/d calculated from oceanographic data. Melting is greatest at depth, above the subglacial channels, causing glacier undercutting. Melt rates increase proportionally to thermal forcing raised to the power of 1.2–1.6 and to subglacial water flux raised to the power of 0.5–0.9. Therefore, in a warmer climate, Store Glacier melting by ocean may increase from both increased ocean temperature and subglacial discharge. **Citation:** Xu, Y., E. Rignot, I. Fenty, D. Menemenlis, and M. Mar Flexas (2013), Subaqueous melting of Store Glacier, west Greenland from three-dimensional, high-resolution numerical modeling and ocean observations, *Geophys. Res. Lett.*, 40, 4648–4653, doi:10.1002/grl.50825.

## 1. Introduction

[2] Mass loss from the Greenland Ice Sheet has increased rapidly in the past decades [Velicogna, 2009] due to a combination of enhanced surface melting and accelerated ice discharge into the ocean [Rignot and Kanagaratnam, 2006; van den Broeke et al., 2009]. Tidewater glaciers dominate the total ice discharge from Greenland to the ocean [Rignot and Mouginot, 2012]. There are indications that many tidewater glaciers accelerated as anomalous warm Atlantic water intruded the glacial fjords [Holland et al., 2008; Hanna et al., 2009; Murray et al., 2010; Christoffersen et al., 2011]. Warm, subsurface ocean waters present in glacial fjords induce high rates of subaqueous melting [Motyka et al., 2003; Rignot et al., 2010; Sutherland and Straneo, 2012; Motyka et al., 2011]. The subaqueous melting of the glacier fronts is fueled by the discharge of subglacial freshwater at

the glacier grounding line. This subglacial discharge results from the collection of surface runoff over the entire glacier drainage basin that reaches the glacier bed through a set of moulins, cracks, and crevasses. Subglacial water is discharged at the glacier grounding line, yields the turbulent, sediment-laden plume that rises quickly along the ice face, entrains ocean heat, and melts ice vigorously [Motyka et al., 2003].

[3] Direct estimates of the melt rate of calving faces are few and subject to large uncertainties. Using conservation of mass, heat, and salinity of the water column, Motyka et al. [2003] calculated a melt rate of 12 m/d for LeConte Glacier, Alaska in the summer of year 2000. Using a similar method, Rignot et al. [2010] derived melt rates ranging from 0.7 to 3 m/d during summer at four tidewater glaciers of West Greenland. Sutherland and Straneo [2012] inferred similarly high melt rates (650 m/yr or 1.8 m/d) for Helheim Glacier, East Greenland.

[4] On the modeling side, a simplified plume model [Jenkins, 2011] and a two-dimensional (2-D) simulation using the Massachusetts Institute of Technology general circulation model (MITgcm) [Xu et al., 2012] revealed the sensitivity of the melt rate to the subglacial water flux and to ocean thermal forcing. The 2-D numerical study of Xu et al. [2012] with grid spacing of 20 m in horizontal and 5 m in vertical, however, did not resolve plume turbulence. Furthermore, Jenkins [2011] and Xu et al. [2012] did not take into account the spatial pattern of subglacial water discharge along the glacier calving face.

[5] Here we resolve the turbulent freshwater plume along the calving face of a tidewater glacier using a three-dimensional (3-D) configuration of the MITgcm with 1 m grid spacing and evaluate the sensitivity of ice melt to the subglacial freshwater flow regime and the thermal forcing from the ocean. We compare the melt rate estimated using oceanographic data with the results of high-resolution simulations and conclude on the importance of ice-ocean interactions for Greenland glaciers.

## 2. Data and Methods

[6] Store Glacier (70°22'N, 50°38'W) is a major tidewater glacier in West Greenland. The glacier is 5 km wide at the ice front, with a draft of about 500 m below sea level. We surveyed the fjord of Store Glacier by boat in August 2010, under calm wind conditions and mild air temperature. A Lowrance 18C sonar depth sounder recorded the fjord bathymetry along the boat track. A hydrographic section of eight stations was collected across the fjord, about 1 km away from the ice front (Figure 1a) using an InterOcean S4 conductivity, temperature, depth, and current profiler

Additional supporting information may be found in the online version of this article.

<sup>1</sup>Earth System Science, University of California, Irvine, California, USA.

<sup>2</sup>Jet Propulsion Laboratory, California Institute of Technology, Pasadena, California, USA.

Corresponding author: Y. Xu, Earth System Science, University of California, 240G Rowland Hall, Irvine, CA 92697, USA. (yunx@uci.edu)

©2013. American Geophysical Union. All Rights Reserved.  
0094-8276/13/10.1002/grl.50825

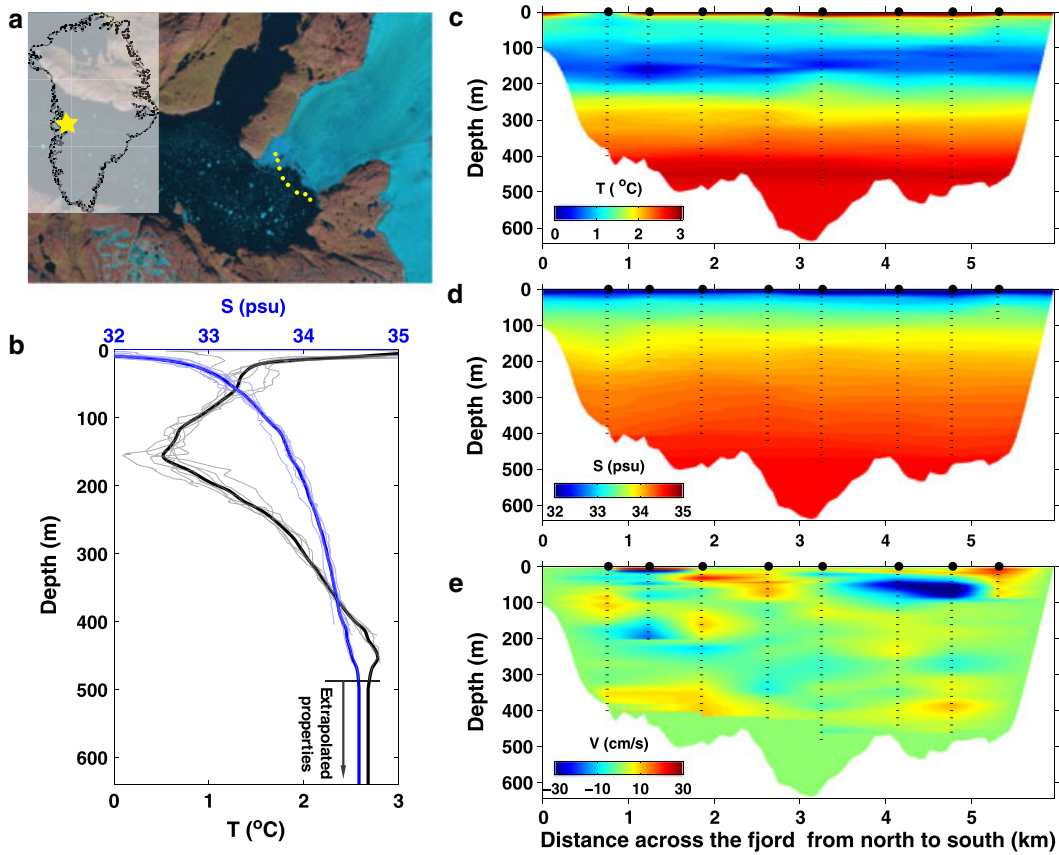


**Figure 1.** (a) LandSat-7 image of Store Glacier fjord with yellow dots at the location of the survey stations in August 2010, (b) T and S profiles (light lines) averaged and extrapolated to the sea floor (bold lines), (c) potential temperature (T), (d) salinity (S), and (e) water speed (V) across the hydrographic section. Positive speed indicates water moving toward the ice. Points below the sea floor are colored white. Each hydrographic station is indicated by a dot in Figures 1c–1e at 0 depth, and dash lines show the depth of the measurements.

(S4, hereafter). The S4 probe measured 30 s averages of temperature ( $\pm 0.02^\circ\text{C}$ ), salinity ( $\pm 0.02$ ), depth ( $\pm 0.15\%$ ), and velocity ( $\pm 0.01$  m/s). The S4 instrument was stationed at discrete depth (5 to 25 m intervals) for 2–3 min to obtain an average velocity at each depth. The velocity data are corrected for boat drift deduced from GPS positioning and projected on the direction perpendicular to the hydrographic section.

[7] We calculate the subaqueous melt rate of Store Glacier by applying the conservation of mass, heat, and salinity to the hydrographic section [Motyka *et al.*, 2003; Rignot *et al.*, 2010]. First, the upper 20 m of the water column is excluded from the calculation for two reasons: (1) the high temperature and low salinity of this layer are primarily due to solar heating and melting of calved ice debris, and therefore, do not provide useful information about subaqueous melting (Figure S2); and (2) the relatively fresh, warm, and therefore stable surface waters do not participate in the melting of ice below the surface. We include an estimating of the error from omitting the upper layer in our error budget. Second, temperature, salinity, and velocity are interpolated and extrapolated across the entire hydrographic section. Extrapolation uses temperature, and salinity profiles (Figure 1b) that are averaged over all eight stations and extrapolated to the sea floor assuming constant values below the depth of our measurements (supporting information). For velocity, we assume

zero velocity along the sidewalls of the fjord (no slip condition). To fill in missing velocity data at depth, we close the salinity budget, i.e., we calculate the residual water velocity that yields zero net salinity flux across the hydrographic section. We find a mean velocity of  $-0.4$  cm/s in the deep area without observations (Figure 1e). Third, assuming that the subglacial freshwater discharge is at the in situ freezing point, we close the heat budget across the hydrographic section to estimate the heat loss due to ice melting and subsequently deduce the corresponding melt rate of the ice face. Finally, we apply the conservation of mass to calculate the subglacial water discharge. More details are given in the supporting information.

[8] To model the melting of the ice face, we use the MITgcm [Marshall *et al.*, 1997a, 1997b], with a free-surface, nonhydrostatic configuration. The three-equation formulation used in Xu *et al.* [2012] to represent the freezing/melting processes on the vertical calving face in 2-D is modified for 3-D simulations (see details in the supporting information).

[9] The model domain is a simplified representation of the Store Glacier fjord, i.e., the sea floor depth is uniform at 500 m and the fjord is rectangular in shape. We simulate a section of the vertical ice face that is 150 m in width ( $y$  axis) by 500 m in height ( $z$  axis), and the ocean domain extends 500 m from the ice face ( $x$  axis). We use 1 m horizontal and

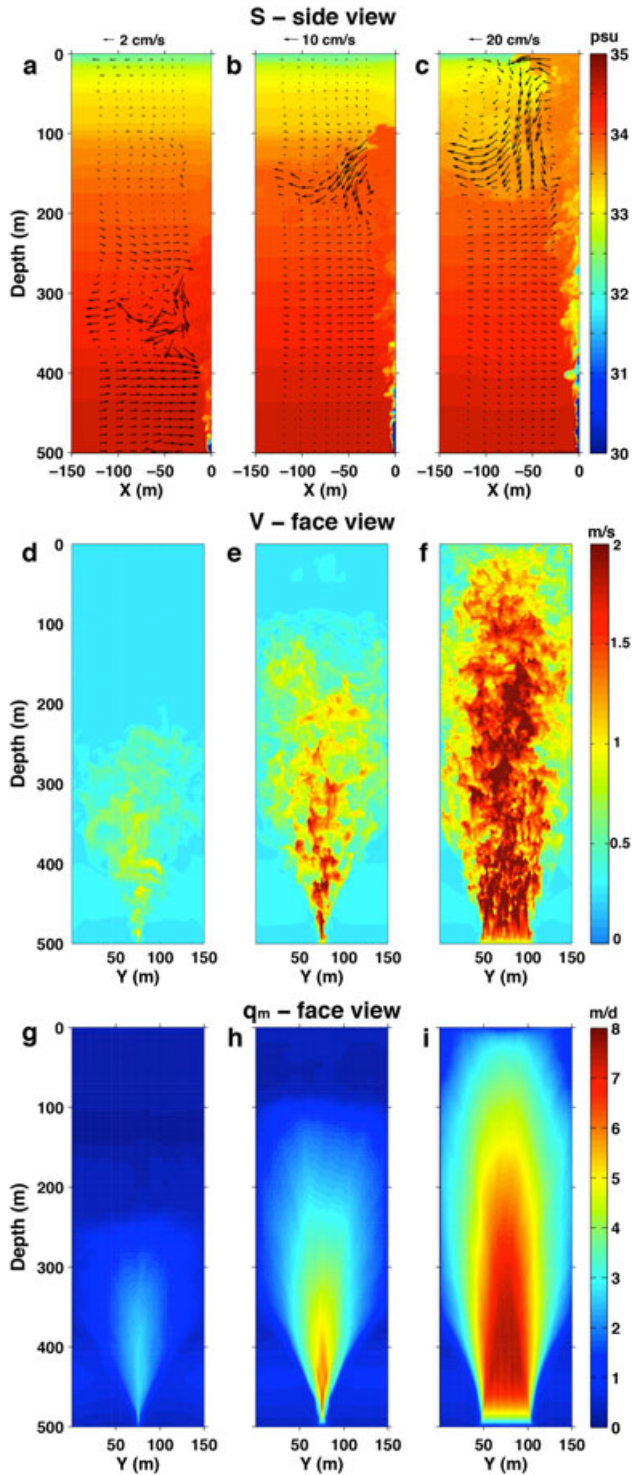


**Figure 2.** 3-D simulations of subglacial freshwater plumes for three-channel configurations and ocean thermal forcing,  $TF = 4.34^{\circ}\text{C}$  as in Figure 1b. (a–c) Side view of the salinity (S), color coded between 30 and 35, with water velocity vectors in the plane of view represented as black arrows; (d–f) face view of water speed (V) adjacent to the ice face; and (g–i) face view of the time-averaged melt rate ( $q_m$ ). The three-channel configurations for subglacial water discharge,  $Q_{sg}$ , are (Figures 2a, 2d, and 2g)  $Q_{sg} = 1 \text{ m}^3/\text{s}$ , channel is 1 m high by 2 m wide; (Figures 2b, 2e, and 2h)  $Q_{sg} = 5 \text{ m}^3/\text{s}$ , channel is 1 m high by 10 m wide; and (Figures 2c, 2f, and 2i)  $Q_{sg} = 30 \text{ m}^3/\text{s}$ , channel is 1 m high by 60 m wide.

vertical grid spacing near the ice front and gradually increase horizontal grid spacing to 5 m in the  $x$  direction at the open ocean boundary. Both the model viscosity and diffusivity are set to  $0.01 \text{ m}^2/\text{s}$ . The Reynolds number,  $Re$ , calculated from the model eddy viscosity is  $\sim 10^4$ . This value is lower than the estimated  $Re \sim 10^8$  of the actual flow in front of the glacier, but it is high enough for the buoyant plume to exhibit turbulence.

[10] We study the evolution of the rate of ice melt as a function of subglacial water flux ( $Q_{sg}$ ) and thermal forcing from the ocean (TF). The subglacial water flux,  $Q_{sg}$ , is estimated using total runoff from the Regional Atmospheric Climate Model (RACMO) [van Angelen *et al.*, 2012]. Ocean thermal forcing, TF, is defined as the difference between the in situ temperature of seawater and its pressure- and salinity-dependent freezing point, averaged between 200 m and 500 m (sea floor). Seawater that participates in the melting of the calving face mainly comes from this depth range, as indicated by the model (Figures 2a–2c). We also investigate the impact of the spatial distribution of  $Q_{sg}$  (supporting information).

[11] To test the sensitivity of the melt rate to  $Q_{sg}$ , we vary  $Q_{sg}$  from 0 to  $45 \text{ m}^3/\text{s}$  along the 150 m long grounding line, which is equivalent to varying  $Q_{sg}$  from 0 to  $1500 \text{ m}^3/\text{s}$  for the entire 5 km wide ice front to be consistent with the RACMO data [van Angelen *et al.*, 2012]. The subglacial water is set to zero salinity and to the pressure- and salinity-dependent freezing point of  $-0.29^{\circ}\text{C}$  at 500 m depth. Subglacial channels at Store Glacier are assumed to have large cross-sectional areas at the terminus and to be low and wide (supporting information). We use a subglacial channel height of 1 m and water speed of 0.5 m/s, and we vary the channel width from 0 to 90 m in order to obtain the above-mentioned range in  $Q_{sg}$  values. Effective subglacial freshwater velocity,  $q_{sg}$ , or  $Q_{sg}$  per unit area of ice front, varies from 0 to 52 m/d in these experiments. We employ two values of TF in these sensitivity experiments with varying  $Q_{sg}$ : (1)  $TF = 4.34^{\circ}\text{C}$  from our oceanographic measurements (Figures 1b); and (2)  $TF = 2^{\circ}\text{C}$ , corresponding to an ocean near  $0^{\circ}\text{C}$ .

[12] To test the sensitivity of the melt rate to ocean thermal forcing, we linearly increase TF by increments of  $1^{\circ}\text{C}$  from  $0^{\circ}\text{C}$  to  $10^{\circ}\text{C}$  and we repeat the simulations for two values of subglacial water flux: (1)  $Q_{sg} = 0$  and (2)  $Q_{sg} = 15 \text{ m}^3/\text{s}$  (equivalent to  $q_{sg} = 0$  and 17 m/d, respectively) for winter and summer conditions.

[13] The salinity data collected near the ice front (Figure 1b) and temperature forcing described above are used to force the model at the open ocean boundary and to initialize the model. Each sensitivity experiment is run for 6 h. This time interval is sufficient to establish statistical equilibrium in the turbulent plume and glacial melt rates.

### 3. Results

[14] The oceanographic data (Figure 1) reveal three major water masses in front of Store Glacier: relatively warm and fresh surface water; cold polar water at intermediate depth; and warm Atlantic water below 300 m depth. From the oceanographic data, we calculate a melt water flux of  $93 \pm 31 \text{ m}^3/\text{s}$ , equivalent to a melt rate of  $3.0 \pm 1.0 \text{ m/d}$  averaged over the entire hydrographic section of  $2.7 \text{ km}^2$ . The subglacial freshwater discharge  $Q_{sg}$  of the entire glacier is estimated at  $246 \pm 45 \text{ m}^3/\text{s}$ . This calculated value compares

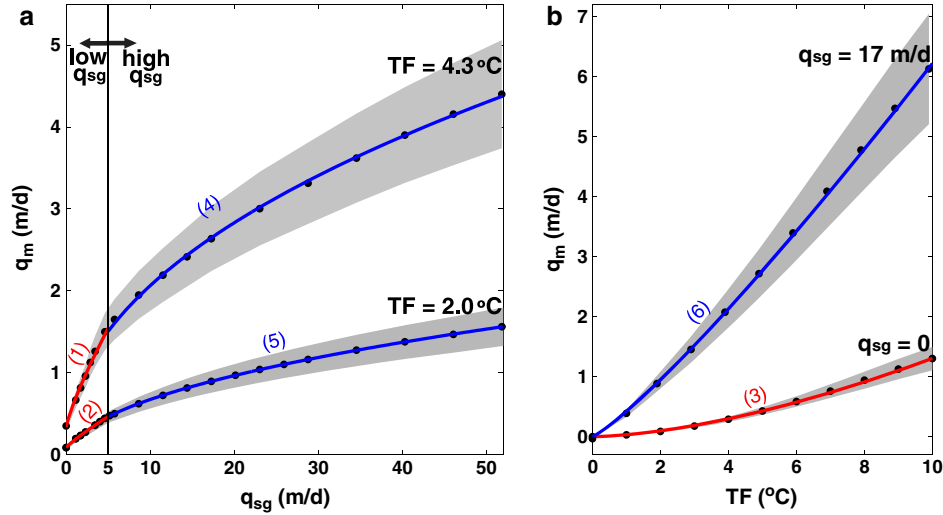


**Figure 3.** Average melt rate,  $q_m$ , in meters per day over the entire ice face versus (a) effective subglacial freshwater velocity,  $q_{sg}$ , in meters per day and (b) ocean thermal forcing TF in degree Celsius. Model results are black dots, with  $\pm 15\%$  error bars indicated by the grey band. We fit the simulated melt rate,  $q_m$ , with an equation of the form  $(A \cdot q_{sg}^\alpha + B)TF^\beta$  for six distinct melt regimes (labeled 1–6). Least squares fit values for  $A$ ,  $B$ ,  $\alpha$ , and  $\beta$  are listed in Table 1. Red and blue curves are model fits for low and high  $q_{sg}$ , respectively.

well with a  $Q_{sg} = 300 \pm 27 \text{ m}^3/\text{s}$  independently deduced from RACMO for August 2010.

[15] Errors in the oceanographic melt estimate result from (1) instrument error in velocity, (2) omission of the surface layers, (3) uncertainties of interpolation and extrapolation of the data, and (4) uncertainties in tidal currents. For (1), the instrument error of velocity is 1 cm/s, yielding an error in melt rate of  $\pm 0.9 \text{ m/d}$  and an error in  $Q_{sg}$  of  $\pm 10 \text{ m}^3/\text{s}$ . For (2), when we vary the depth of omitted surface layers from 10 m to 30 m, the melt rate varies by  $\pm 0.2 \text{ m/d}$  and  $Q_{sg}$  varies by  $43 \text{ m}^3/\text{s}$ . For (3), if the uncertainty of the velocity at each grid point is 12.8 cm/s, that is, the standard deviation of all velocity measurements, the uncertainty in melt rate is  $\pm 0.3 \text{ m/d}$  and in  $Q_{sg}$  is  $\pm 6 \text{ m}^3/\text{s}$ . For (4), tidal currents estimated from the tidal model of *Padman and Erofeeva* [2004] are only  $\pm 0.01 \text{ cm/s}$  at the location of our boat survey, therefore negligible. Taking all these errors into account, we obtain a total error of  $\pm 1.0 \text{ m/d}$  for the melt rate and  $\pm 45 \text{ m}^3/\text{s}$  for  $Q_{sg}$ .

[16] Figure 2 shows that following the release of buoyant subglacial water at the grounding line, the ascending flow quickly transitions to turbulence. As the turbulent plume rises, it entrains ambient seawater and expands laterally. It eventually reaches neutral buoyancy at some intermediate depth and flows horizontally away from the ice wall. The melt rate is highest along a fan-shaped region immediately above the subglacial channel where turbulent mixing is most effective and decreases away from the plume core. For  $TF = 4.34^\circ\text{C}$  and low  $Q_{sg}$  ( $1 \text{ m}^3/\text{s}$ ), the plume reaches neutral buoyancy at 320 m depth, where it spreads laterally over the entire model domain. The maximum melt rate exceeds 2 m/d, and the area-average melt rate is 0.66 m/d for the entire submerged ice face. At high  $Q_{sg}$  ( $5 \text{ m}^3/\text{s}$ ), the subglacial plume reaches neutral buoyancy at 160 m depth but rises up to 100 m due to inertia before sinking back to its level of neutral buoyancy. The plume occupies the entire model domain above 300 m depth. The maximum melt rate

is 6 m/d, and the average melt rate is 0.96 m/d. At very high  $Q_{sg}$  ( $30 \text{ m}^3/\text{s}$ ), the plume reaches neutral buoyancy at 100 m depth and some fraction of the plume upwells to the surface before sinking back to neutral buoyancy. The maximum melt rate is 8 m/d, and the average melt rate is 3.6 m/d.

[17] The average melt rate increases when the subglacial freshwater flux increases and when ocean thermal forcing increases (Figure 3). When  $q_{sg} = 0$ , the average melt rate is 0.35 m/d for  $TF = 4.34^\circ\text{C}$  and 0.09 m/d for  $TF = 2^\circ\text{C}$ . When  $TF = 0^\circ\text{C}$ , the melt rate is 0 for all values of  $q_{sg}$ . We therefore use the approximate fit of the simulated melt rate ( $q_m$ ) as a function of  $q_{sg}$  and TF as

$$q_m = (A \cdot q_{sg}^\alpha + B) \cdot TF^\beta \quad (1)$$

In our simulations (Figure 3a), we distinguish two melt regimes: (1)  $q_{sg} > 5 \text{ m/d}$  and (2)  $q_{sg} < 5 \text{ m/d}$ . The best model fit is achieved with the parameter values listed in Table 1. Model fit residuals are less than 0.05 m/d. Changes in the shape of the subglacial channels introduce an uncertainty in melt rate of about 15% (Figure S3), which is the level of uncertainty indicated by the shaded regions in Figure 3.

**Table 1.** Parameters of Equation (1) That Provide the Best Fit to Simulated Melt Rates for the Six Melt Regimes Identified in Figure 3

		A	$\alpha$	B	$\beta$
Low $q_{sg}$	(1)	0.030	0.85	0.031	1.61
	(2)	0.030	0.88	0.029	1.61
	(3)	/	/	0.032	1.61
High $q_{sg}$	(4)	0.083	0.54	0.081	1.17
	(5)	0.075	0.55	0.038	1.17
	(6)	0.075	0.54	0.07	1.17

#### 4. Discussion

[18] The numerical experiments with the MITgcm aim to resolve the subglacial plume in front of a glacier with an ocean general circulation model in 3-D and at high spatial resolution. The simulated turbulent plume spreads laterally and expands rapidly to the entire lateral domain (Figure 2). This is a characteristic that was not reproduced in 2-D simulations [Xu *et al.*, 2012].

[19] The model indicates that subaqueous melting is unevenly distributed: it is highest above the subglacial channels and negligible near the surface. This process will tend to carve ice faces into ice cliffs slanted outward, hence undercutting the glacier face. Observations of the shape of the glacier front would be of interest to confirm this prediction. Meanwhile, ice face undercutting may explain a dominant form of calving observed in the field [Motyka *et al.*, 2003]. This melt pattern also implies that ice melting by the ocean will directly affect the position of the glacier grounding line. In particular, a higher rate of ice melting will remove ice at depth and result in grounding line retreat unless melting is compensated by the advection of ice from upstream.

[20] The numerical experiments indicate a high sensitivity of the melt rate to ocean thermal forcing. The main driver of the change in ice melting is ocean temperature a few hundred meters below the surface, where our oceanographic data reveal the presence of warm, salty, Atlantic water, and where the numerical simulations reveal an iceward flow driven by the convection of freshwater plumes.

[21] Subglacial freshwater discharged at the grounding line accelerates the convection-driven circulation at the glacier front, increases the heat flux to the ice, and results in higher melt rates. Subglacial water is the direct product of surface runoff in the glacier drainage basin. As climate warms, and more ice and snow melts at the surface of Greenland, the glacier front will experience enhanced ice melting even if the ocean temperature in the fjord is held constant.

[22] The results of our sensitivity experiment are consistent with the 2-D experiments of Xu *et al.* [2012] and the simplified plume model of Jenkins [2011]. But our 3-D results suggest a more complicated dependence of  $q_m$  on  $q_{sg}$  and TF than in these prior studies. In particular, the melt rate becomes less sensitive to  $q_{sg}$  and TF at high  $q_{sg}$ .

[23] As stated in equation S7, the melt rate is proportional to the product of TF and the heat transfer rate of water along the ice face. The heat transfer rate may increase with TF, because at higher TF, more melt water is produced and added to the buoyant water plume and increases water velocity. The combined effect of enhanced TF and entrainment rate explains the simulated nonlinear increase of  $q_m$  with TF. When  $q_{sg}$  is low, we find that  $q_m$  is sensitive to  $TF^{1.6}$ . The sensitivity decreases to  $TF^{1.2}$  at high  $q_{sg}$ , because at high  $q_{sg}$ , the buoyant plume is dominated by  $q_{sg}$  and the heat transfer rate becomes less sensitive to the increase in  $q_m$ .

[24] Similarly,  $q_m$  is proportional to  $q_{sg}^{0.8}$  for low  $q_{sg}$  and to  $q_{sg}^{0.5}$  for high  $q_{sg}$ . We explain this as follows. At  $q_{sg} = 5$  m/d, the plume reaches buoyancy equilibrium with the surrounding water at about 150 m depth. When  $q_{sg}$  increases further, the expansion of the plume slows down and so does the ice-plume contact area. This transition in response of  $q_m$  to  $q_{sg}$  is likely dependent on ocean stratification and glacier geometry and therefore may occur at different values of  $q_{sg}$  for different stratifications and geometries.

[25] The simulated melt rate is  $2.0 \pm 0.3$  m/d for Store Glacier during August 2010, when  $TF = 4.34^\circ\text{C}$  and  $q_{sg} = 10$  m/d (Figure 3). This value is lower than the  $3.0 \pm 1.0$  m/d melt rate inferred from ocean measurements, yet within measurement errors. This comparison is not sufficient to evaluate the model or refine its controlling parameters. To refine the comparison between model and observations, more complexities of the fjord/glacier configuration and the subglacial freshwater flow regime must be considered in numerical modeling, and additional oceanographic data collected over longer time periods are needed.

[26] An approximate dependence of the subaqueous melt rate on ocean temperature and subglacial discharge for Store Glacier is given by equation (1), which can be used to estimate the seasonal and/or multiple-year melt rates of Store Glacier if long-term TF and  $Q_{sg}$  data are available. However, this relationship will likely not hold for other tidewater glaciers with different glacier and fjord geometry and ocean stratification, i.e., new simulations will be needed.

[27] Ocean temperature varies by less than  $0.5^\circ\text{C}$  in Store Glacier fjord between summer and winter [Rignot *et al.*, 2012] or by similarly low values in other glacier fjords [Straneo *et al.*, 2010], while  $Q_{sg}$  changes from near zero in winter to hundreds of  $\text{m}^3/\text{s}$  in summer according to RACMO. Based on equation (1), the melt rate is 1 order of magnitude lower in winter compared to summer. The melting of submerged ice faces in Greenland should therefore exhibit a strong seasonality, even if the subsurface waters do not exhibit a strong seasonality in temperature.

[28] The parameterization of ice-ocean boundary processes depends on the heat/salinity transfer rates. Here we use the parameterization of Jenkins *et al.* [2010], which is based on seawater temperature measured 1.9 m from the ice and current speed measured 20 m from the ice. We use these coefficients in the first wet grid cell next to the ice, i.e., within 1 m from the ice. This is reasonable and compatible with the parameterization of Jenkins *et al.* [2010] because our turbulent plume is well mixed in that region. The reasonable agreement between simulated melt rate and that derived from oceanographic data suggests that the heat and salinity transfer coefficients in the model are of the right order of magnitude. In future studies, however, it would be important to better constrain the values of these parameters.

[29] The velocity of Store Glacier is about 13 m/d at the terminus [Rignot and Mouginot, 2012]. Our calculated melt rates indicate that melting of ice by the ocean removes 20% of the glacier influx, i.e., that 80% must be removed by iceberg calving. Part of the ice removed from calving, however, will be affected by glacier undercutting caused by ice-ocean interactions. It is therefore difficult to estimate the exact partitioning between melting and calving processes in controlling the position of the ice front. Our model results suggest that in the case of Store Glacier, the dominant mode of ice removal at the ice front is iceberg calving.

#### 5. Conclusion

[30] In this study, we model the melting of Store Glacier using a high-resolution ocean general circulation model and we compare the results with oceanographic data. We obtain a reasonable agreement between model and observations. In addition, the numerical experiments indicate that the melt rate varies significantly with subglacial water flux and

with ocean temperature; but the sensitivity decreases at high subglacial water fluxes. These results provide simple guidelines for the inclusion of ice-ocean interactions along the calving fronts of Greenland glaciers in ice sheet numerical models and for interpreting recent changes in glacier fronts as a result of enhanced surface runoff or intrusion of warm Atlantic waters in the glacial fjords. To improve our understanding of ice-ocean interactions, however, additional oceanographic observations are critically needed, in particular, to better constrain the in situ estimation of melt rates, the distribution and geometry of subglacial water channels, and the details of the fjord bathymetry and shape of the calving face, along with longer term and more detailed measurements of ocean conditions within the fjords.

[31] **Acknowledgments.** We thank Roman Motyka and an anonymous reviewer for their constructive comments. We thank Jan H. van Angelen and Michiel R. van den Broeke (Utrecht University) for providing the daily RACMO runoff data. This work was performed at the University of California Irvine under a contract with the National Aeronautics and Space Administration Cryosphere Science Programs.

[32] The Editor thanks Roman Motyka for his assistance in evaluating this paper.

## References

- Christoffersen, P., R. Mugford, K. Heywood, I. Joughin, J. Dowdeswell, J. Syvitski, A. Luckman, and T. Benham (2011), Warming of waters in an east Greenland fjord prior to glacier retreat: Mechanisms and connection to large-scale atmospheric conditions, *The Cryosphere*, 5(3), 701–714.
- Hanna, E., J. Cappelen, X. Fettweis, P. Huybrechts, A. Luckman, and M. Ribergaard (2009), Hydrologic response of the Greenland ice sheet: The role of oceanographic warming, *Hydrol. Process.*, 23(1), 7–30.
- Holland, D. M., R. H. Thomas, B. De Young, M. H. Ribergaard, and B. Lyberth (2008), Acceleration of Jakobshavn Isbrae triggered by warm subsurface ocean waters, *Nat. Geosci.*, 1(10), 659–664, doi:10.1038/ngeo316.
- Jenkins, A. (2011), Convection-driven melting near the grounding lines of ice shelves and tidewater glaciers, *J. Phys. Oceanogr.*, 41(12), 2279–2294.
- Jenkins, A., K. W. Nicholls, and H. F. J. Corr (2010), Observation and Parameterization of Ablation at the Base of Ronne Ice Shelf, Antarctica, *J. Phys. Oceanogr.*, 40(10), 2298–2312, doi:10.1175/2010JPO4317.1.
- Marshall, J., A. Adcroft, C. Hill, L. Perelman, and C. Heisey (1997a), A finite-volume, incompressible Navier Stokes model for studies of the ocean on parallel computers, *J. Geophys. Res.*, 102(C3), 5753–5766, doi:10.1029/96JC02775.
- Marshall, J., C. Hill, L. Perelman, and A. Adcroft (1997b), Hydrostatic, quasi-hydrostatic, and nonhydrostatic ocean modeling, *J. Geophys. Res.*, 102(C3), 5733–5752, doi:10.1029/96JC02776.
- Motyka, R., L. Hunter, K. Echelmeyer, and C. Connor (2003), Submarine melting at the terminus of a temperate tidewater glacier, LeConte Glacier, Alaska, USA, *Ann. Glaciol.*, 36, 57–65.
- Motyka, R. J., M. Truffer, M. Fahnestock, J. Mortensen, S. Rysgaard, and I. Howat (2011), Submarine melting of the 1985 Jakobshavn isbræ floating tongue and the triggering of the current retreat, *J. Geophys. Res.*, 116, F01007, doi:10.1029/2009JF001632.
- Murray, T., et al. (2010), Ocean regulation hypothesis for glacier dynamics in southeast Greenland and implications for ice sheet mass changes, *J. Geophys. Res.*, 115(F03026), doi:10.1029/2009JF001522.
- Padman, L., and S. Erofeeva (2004), A barotropic inverse tidal model for the arctic ocean, *Geophys. Res. Lett.*, 31, L02303, doi:10.1029/2003GL019003.
- Rignot, E., and P. Kanagaratnam (2006), Changes in the velocity structure of the Greenland ice sheet, *Science*, 311, 986–990.
- Rignot, E., and J. Mouginot (2012), Ice flow in Greenland for the international polar year 2008–2009, *Geophys. Res. Lett.*, 39, L11501, doi:10.1029/2012GL051634.
- Rignot, E., I. Fenty, D. Menemenlis, and Y. Xu (2012), Spreading of warm ocean waters around Greenland as a possible cause for glacier acceleration, *Ann. Glaciol.*, 53(60), 257–266.
- Rignot, E., M. Koppes, and I. Velicogna (2010), Rapid submarine melting of the calving faces of West Greenland glaciers, *Nat. Geosci.*, 3(3), 187–191, doi:10.1038/NNGEO765.
- Straneo, F., G. S. Hamilton, D. A. Sutherland, L. A. Stearns, F. Davidson, M. O. Hammill, G. B. Stenson, and A. Rosing-Asvid (2010), Rapid circulation of warm subtropical waters in a major glacial fjord in East Greenland, *Nat. Geosci.*, 3(3), 182–186, doi:10.1038/NNGEO764.
- Sutherland, D. A., and F. Straneo (2012), Estimating ocean heat transports and submarine melt rates in Sermilik Fjord, Greenland, using lowered acoustic doppler current profiler (ladcp) velocity profiles, *Ann. Glaciol.*, 53(60), 50–58.
- van Angelen, J., J. Lenaerts, S. Lhermitte, X. Fettweis, P. Kuipers Munneke, M. van den Broeke, and E. van Meijgaard (2012), Sensitivity of Greenland ice sheet surface mass balance to surface albedo parameterization: A study with a regional climate model, *The Cryosphere*, 6, 1175–1186.
- van den Broeke, M., J. Bamber, J. Ettema, E. Rignot, E. Schrama, W. J. van de Berg, E. van Meijgaard, I. Velicogna, and B. Wouters (2009), Partitioning recent Greenland mass loss, *Science*, 326(5955), 984–986, doi:10.1126/science.1178176.
- Velicogna, I. (2009), Increasing rates of ice mass loss from the Greenland and Antarctic ice sheets revealed by GRACE, *Geophys. Res. Lett.*, 36, L19503, doi:10.1029/2009GL040222.
- Xu, Y., E. Rignot, D. Menemenlis, and M. Koppes (2012), Numerical experiments on subaqueous melting of Greenland tidewater glaciers in response to ocean warming and enhanced subglacial discharge, *Ann. Glaciol.*, 53(60), 229–234.